Mid-IR Super-Continuum Generation

Mohammed N. Islam*[a,b], Chenan Xia[a], Mike J. Freeman[b], Jeremiah Mauricio[b], Andy Zakel[b], Kevin Ke[a], Zhao Xu[a], and Fred L. Terry, Jr.[a]
[a]Department of Electrical Engineering and Computer Science, University of Michigan, Ann Arbor, MI 48109-2122
[b]Omni Sciences, Inc., 647 Spring Valley Drive, Ann Arbor, Michigan 48105-1060

ABSTRACT

A Mid-InfraRed FIber Laser (MIRFIL) has been developed that generates super-continuum covering the spectral range from 0.8 to 4.5 microns with a time-averaged power as high as 10.5W. The MIRFIL is an all-fiber integrated laser with no moving parts and no mode-locked lasers that uses commercial off-the-shelf parts and leverages the mature telecom/fiber optics platform. The MIRFIL power can be easily scaled by changing the repetition rate and modifying the erbium-doped fiber amplifier. Some of the applications using the super-continuum laser will be described in defense, homeland security and healthcare. For example, the MIRFIL is being applied to a catheter-based medical diagnostic system to detect vulnerable plaque, which is responsible for most heart attacks resulting from hardening-of-the-arteries or atherosclerosis. More generally, the MIRFIL can be a platform for selective ablation of lipids without damaging normal protein or smooth muscle tissue.

Keywords: Fiber Laser, Mid-Infrared, Supercontinuum, Biophotonics, Atherosclerosis, Infrared Countermeasures

1. INTRODUCTION

Supercontinuum (SC) generation process, in which the spectrum of a narrow bandwidth laser undergoes a substantial spectral broadening through the interplay of different nonlinear optical interactions, has been widely reported and studied since it was observed in 1969 [1]. Recently, broadband SC generation in optical fibers is of particular interest because of the optical fibers' unique advantages in their long optical interaction length, high nonlinearity, and potential applications in the optical telecommunication [2], [3]. For example, a soft-glass (Schott SF6) photonics crystal fiber (PCF) has been used to generate and extend the SC spectrum down to ~350 nm in the deep blue regime [4]. Also, various techniques have been used to demonstrate SC generation with the long wavelength edge reaching as far as ~3 μm [4], [5], which is then limited by the soaring material absorption of the silica glass [6]. Recently, the time-averaged power of the SC in the PCF fiber has also been increased to 50 W [7].

A high power all-fiber-integrated mid-IR SC light source has applications in a variety of areas. Conventional mid-IR laser sources, including optical parametric amplifiers (OPA) [8], quantum cascaded lasers [9], synchrotron lasers [10], and free electron lasers [11], are used in infrared countermeasures [9], free-space communications [9], and optical tissue ablation [12]. In comparison, SC lasers have no moving parts, output in single spatial mode and operate at room temperature. In addition, fiber-based SC source can generate a broad spectrum covering the entire near- and mid-IR regime simultaneously, which can improve both the sensitivity and selectivity of remote chemical sensing [13], and real-time optical metrology [14]. Finally, direct signal modulation functionality is also desirable for SC laser sources to eliminate the need for external signal modulation or chopping equipments, which is difficult to implement in the mode-locked lasers based systems [15], [16].

To generate SC spectrum in the mid-infrared (mid-IR), optical fibers with low loss in the mid-IR windows, such as chalcogenide, fluoride, and tellurite, are required. For example, spectrum shifting from 1.55 μm to ~1.9 μm is reported in the chalcogenide fibers, where further wavelength red-shifting is limited due to the low optical damage threshold of ~1 GW/cm^2 and high normal dispersion [17]. SC generation ranging from 2-3 μm has also been demonstrated in sulfide and

* mni@umich.edu; phone 734-647-9700; fax 734-763-9324

Fiber Lasers VI: Technology, Systems, and Applications, edited by Denis V. Gapontsev, Dahv A. Kliner, Jay W. Dawson, Kanishka Tankala, Proc. of SPIE Vol. 7195, 71950W
 · doi: 10.1117/12.807206

selenide fibers by a 2.5 μm OPA pump laser [18]. On the other hand, mode-locked femtosecond lasers have been used to generate SC spectrum beyond 3 μm in both fluoride [15] and tellurite fibers [16] with modest average power (<0.1 W). We have also developed a ZBLAN (ZrF_4-BaF_2-LaF_3-AlF_3-NaF) fluoride fiber based laser source to provide a SC spectrum ranging from ~0.8 μm to ~4.5 μm [19], and we have scaled up the time-averaged output power to 1.3 W by using cladding-pumped fiber amplifiers in a table-top system [20].

In this paper, we describe an all-fiber-integrated SC laser that can provide a time-averaged output power scalable up to 10.5 W in the mid-IR with direct pulse pattern modulation capability. The SC extends beyond 4 μm in ZBLAN fibers with an average output power of 10.5 W—the highest SC power reported to date in the mid-IR fibers. In addition, the average output power of the SC laser is linearly scalable with respect to the total pump power by varying the pulse duty cycle while maintaining the similar spectral shape. For the first time to our knowledge, we also demonstrate pulse pattern modulation of the SC by directly modulating the seed laser diode and controlling the amplifier gain with signal feedback technique. Our SC laser can output a modulated pulse pattern with the duty cycle adjustable from nominally 0% to 100%. Therefore, our SC laser has no moving parts, covers the near- and mid-IR spectrum, and eliminates the need for mode-locked lasers.

The pump system of the SC laser comprises a 1542 nm laser diode generating 1 ns pulses, followed by a single mode erbium doped fiber amplifier (EDFA) and multi-stage cladding-pumped erbium/ytterbium co-doped fiber amplifiers (EYFA). Optical spectrum of the amplified nanosecond pulses is then broadened in a combination of 2 m length of standard single mode fiber (SMF) followed by 7 m length of ZBLAN fiber. Numerical simulations are also carried out to investigate the power and spectral bandwidth limit of the SC generation in ZBLAN fluoride fibers.

This paper is organized as follows. We describe the SC laser setup in section 2 and experimental results of the SC generation in section 3. We demonstrate, in section 4, the pulse pattern modulation of our SC laser. In section 5, as one example of the application of the SC we use wavelengths between 2.6 and 3.8 microns to identify and selectively ablate lipids and proteins. In particular, absorption spectroscopy and selective ablation are conducted on atherosclerotic plaque constituents and adipose/fat tissues. Finally, we discuss and summarize the experimental and simulation results in Section 6.

2. EXPERIMENTAL SETUP

The experimental setup is illustrated in Fig. 1. A 10 mW distributed feedback (DFB) laser diode emitting at 1542 nm is driven by electronic circuits to provide 400 ps to 2 ns pulses at variable repetition rate. The electronic circuits can also drive the laser diode to output a pre-programmed pulse pattern instead of fixed repetitive pulses. Details of the pulse pattern modulation will be described in Section 4. The optical pulses are amplified by three stages of fiber amplifiers—an EDFA pre-amplifier followed by EYFA mid-stage and power amplifiers. The pre-amplifier uses a 1 meter length of 4/125 μm (core/cladding diameter) single mode erbium doped gain fiber, and the mid-stage amplifier employs a 1.5 meter length of 7/125 (core/cladding diameter) cladding-pumped gain fiber. In a multi-stage amplifier, the noise performance, i.e. amplified spontaneous emission (ASE), is determined by the upstream stages before the power amplifier. To lower the ASE, we separate the amplifier into one pre-amplifier and one mid-stage amplifier. Therefore, the ASE after the first stage can be filtered by a 100 GHz bandpass filter, and the signal gain in each amplifier stage can be reduced. Optical isolators are also placed between the stages to protect the system from back-reflection damage as well as reduce the noise figure and improve the efficiency of the combined amplifier system. Under typical operating conditions, we obtain ~20 dB gain in both the pre- and mid-amplifier for the optical signal while the ASE-to-signal ratio is measured to be less than 1%. The nonlinear broadening of the optical pulses before the power amplifier is also negligible. In addition, a 1% optical tap is used to sample the output power of the pre-amplifier and to enable the signal feedback control, which is described in detail in Section 4.

The power from the mid-amplifier is boosted in an all-fiber-spliced, cladding-pumped, EYFA before coupling into the SC fiber. A cladding-pumped fiber amplifier is required to increase the gain volume and enable the coupling of multiple pump diodes. In addition, to minimize the nonlinear effects in the amplifier, a short length of gain fiber with a large core diameter and a high doping concentration is used. For the 10 W SC generation experiment, we have designed a gain fiber with a core diameter of 15 μm and an effective NA of 0.15, whose mode field is close to that of the SMF fiber. The EYFA has a ~5 m length of gain fiber with a 15/200 μm core/cladding diameter and a 2 dB/m absorption at 915 nm. Ten 8 W 976 nm and two 8 W 940 nm uncooled multimode pump diodes are coupled into the gain fiber through an 18×1

pump combiner. Single spatial mode operation is maintained in the EYFA by carefully splicing the gain fiber to the signal-input SMF fiber and the pump combiner. By pumping the system with ~75 W average power in the counter-propagation configuration, the EYFA can provide ~20.2 W average power output after a 2 m length of SMF fiber that is spliced to the output of the gain fiber. This corresponds to ~6.1 kW peak power (~15 dB signal gain) for 1 ns pulses at a 3.33 MHz repetition rate and ~27% pump-to-signal conversion efficiency. The output spectrum after the SMF fiber is broadened and red-shifted to ~2.2 μm primarily due to the break-up of the nanosecond pulses through modulation instability (MI) followed by soliton self-frequency shifting [5]. The pump-to-signal conversion efficiency is slightly lower than the usual 30-35% figure because of the high peak power induced nonlinear wavelength generation in both the fiber amplifier and single mode fiber.

For the SC modulation experiment, we use a 12/130 μm core/cladding diameter erbium/ytterbium co-doped fiber with a 0.20 NA as the gain fiber in the final stage power amplifier. We reduce the length of the gain fiber to ~4 m because the 940 nm pump cladding absorption is increased to ~3.3 dB/m. Four 6 W, 940 nm pump diodes are coupled into the gain fiber through a 6×1 pump combiner. We generate ~6 W (~10 kW) average(peak) output power after ~2 m length SMF fiber when the seed laser is operated at 1.54 MHz repetition rate with ~400 ps pulse duration.

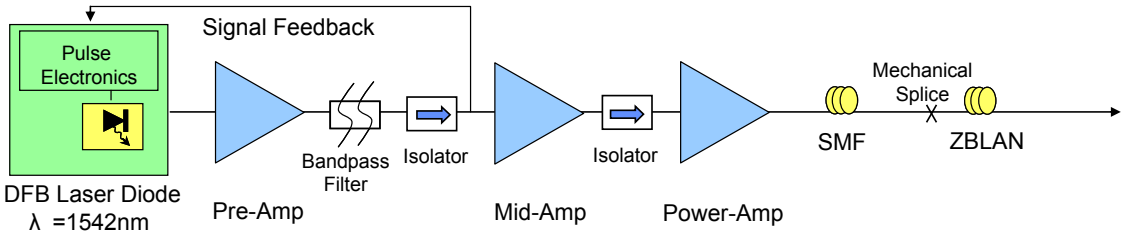

Fig.1. High power all-fiber-integrated SC laser setup.

We generate the SC in a two-stage process. In the first stage SMF fiber, we utilize modulation instability (MI) to break up the nanosecond pulses into femtosecond pulse trains to enhance the nonlinear optical effects and red-shift the optical spectrum to beyond 2 μm [5]. The SC spectrum is then broadened in the following ZBLAN fiber through the interplay of self-phase modulation, Raman scattering and parametric four-wave mixing [5], [20].

SC is generated by butt coupling the light from the 2 m length of SMF fiber after the EYFA into a piece of ZBLAN fluoride fiber. Two ZBLAN fluoride fibers are used in the experiments. In the 10.5 W high power SC experiment, the ZBLAN fiber we designate as FL#1 is 7 m long and has a core diameter of 8.9 μm, a cladding diameter of 125 μm and an NA of 0.21. The ZBLAN fiber we call as FL#2 is used in the SC modulation experiment has a length of ~15 m with a core diameter of 10.6 μm, a cladding diameter of 125 μm and an NA of 0.2. All ends of SMF and ZBLAN fibers are angle-cleaved to avoid light back reflected into the pump system. To improve the coupling stability and heat dissipation capacity, each end of the butt-coupling fibers, i.e. SMF and ZBLAN fibers, is mechanically clamped onto an aluminum v-groove and the fiber claddings are covered with a high refractive index optical glue to remove the residual cladding modes. The SC spectrum between 500 nm and 1750 nm is measured by an optical spectral analyzer, while the spectral information ranging from 1750 nm to 4500 nm is acquired using a Czerny-Turner monochromator and a liquid nitrogen cooled InSb detector..

3. 10.5 W SC GENERATION IN ZBLAN FIBERS

Mid-IR SC with a time-averaged power of 10.5 W and a continuous spectrum of ~0.8 to more than 4 μm is generated by pumping a ~2 m length of SMF fiber followed by ~7 m length of ZBLAN fluoride fiber (FL#1) with the amplified nanosecond pulses as illustrated in Fig. 2. The generated SC is smooth and relatively flat across the majority of the spectrum with a spectral power density >0 dBm/nm (1 mW/nm). The measured SC spectrum is corrected for the spectral responsivity of the InSb detector. The spectral power density is then calculated by using the total SC output power measured by the thermal power meter. The pump to SC conversion efficiency in the ZBLAN fiber is >50%, i.e. 10.5 W of SC output / 20.2 W out of the SMF fiber. The SC average power beyond 1600 nm, 2500 nm, and 3000 nm is measured to be ~7.3 W, ~3.0 W and ~1.1 W, respectively, by using long pass filters with the corresponding cut-off

wavelengths. The residual power in the 1550 nm pump wavelength is less than 0.1 W. The average power of the SC is currently limited by the available pump power from the fiber amplifiers. The long wavelength edge of the SC is primarily limited by the length of the ZBLAN fiber in conjunction with other optical effects, including the fiber bend-induced loss and ZBLAN material absorption [19], [20].

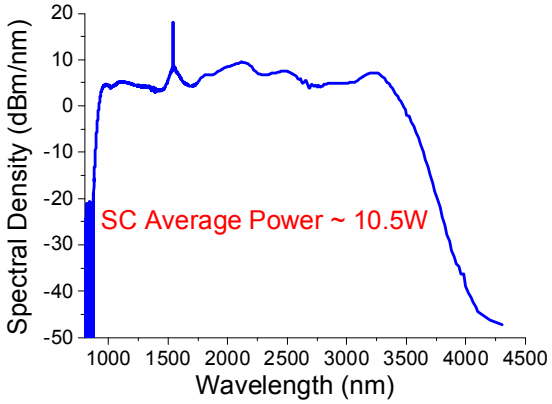

Fig. 2. SC Spectrum for 2m SMF followed by ~7m ZBLAN fiber (FL#1).

For a given fiber, there are three adjustable parameters in our SC light source, which are pulse width, repetition rate and pump power. To obtain the maximum SC power in the mid-infrared and generate the broadest spectrum, all three parameters should be optimized. The laser pulse width is set based on the following two criteria. First, the pulse width shall be short enough to mitigate any transient thermal effects in the optical fiber. On the other hand, a nanosecond pulse scale is also preferable for the intra-pulse nonlinear interaction and spectrum broadening. Therefore, we drive our DFB laser diode with the pulse width in the range of 0.4-2 ns. Furthermore, the pulse repetition rate couples with the pulse width to determine the duty cycle of the laser system. Since the DFB laser diode pulses remove the energy provided by the EYFA pump lasers of the power amplifier of the SC system in the time between DFB pulses, the peak output power varies inversely with the pulse duty cycle with a fixed pump power supply. In other words, the peak output power increases with the reduction of the pulse repetition rate, i.e. pulse duty cycle, and vice versa.

Figure 3 shows the average power of SC spectral components beyond 3000 nm for varying pulse repetition rate with four 976 nm pump diodes. As can be seen, the total SC spectral power beyond 3000 nm increases from ~0.19 W to ~0.48 W by reducing the pulse repetition rate from 1.33 MHz to 0.67 MHz. We attribute the increase of spectral power to the boost of the peak power coupled into the SMF and ZBLAN fibers to enhance the nonlinear SC generation process [5], [20]. However, the SC power beyond 3000 nm drops down to ~0.26 W when we further decrease the repetition rate 0.25 MHz. The drop of the SC spectral power can be caused by the increased power loss in the SC long wavelength edge and reduced amplifier conversion efficiency in the low duty cycle operational condition. Since the SC long wavelength edge is limited by the loss of the fiber, including both bend-induced loss and fluoride material loss, the additional spectrum generated in the vicinity of the SC edge by the additional peak power is heavily attenuated, which in turn reduces the total SC power in the mid-IR regime. In other words, despite of the fact that higher peak power could lead to more spectral broadening, such spectral components vanish during their propagation in the ZBLAN fiber and are not observed at the output end. Therefore, the SC light source should be operated at the repetition rate of 0.67 MHz in this particular case to achieve the maximum spectral output in the mid-IR.

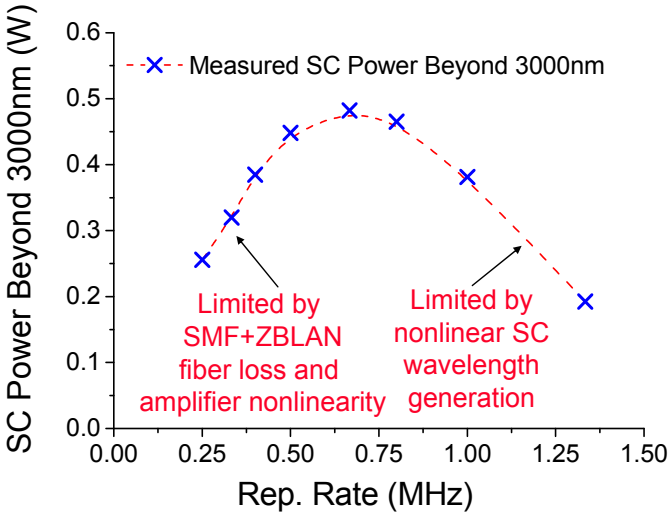

Fig. 3. Average power of SC spectral components beyond 3000 nm for varying pulse repetition rate with four 976 nm pump diodes.

The time-averaged power of SC is linearly scalable with respect to the input pump power without changing the spectral shape. Since the entire SC spectrum is generated in each amplified nanosecond laser pulse, which does not interact with adjacent optical pulses, the SC average power can be boosted by simply increasing the total number of the optical pulses in the given time period. To ensure the SC spectral shape is maintained, the peak power of the amplified pulses are kept the same by adjusting the pulse repetition rate and total pump power for the fiber amplifiers. As illustrated in Fig. 4a, we scale the SC average power from 1.4 W to 10.5 W by varying the pulse repetition rate proportionally from 0.42 MHz to 3.33 MHz and increasing the pump power accordingly. The change of the SC average is linearly proportionally to the change of the pulse duty cycle, which agrees well with our hypothesis. To further confirm that the same SC spectrum shape has been generated under during the change of the SC average power, the ratio of the SC spectral power beyond 2500 nm over the total SC power is measured and shown in Fig. 4b. We observe that the ratio stays approximately constant across the entire power range, which indicates that the power generated in the mid-IR scales up proportionally to the increasing total SC power. Therefore, the output power of our SC light source can be linearly and continuously varied with respect to the input pump power while keeping the same spectral shape.

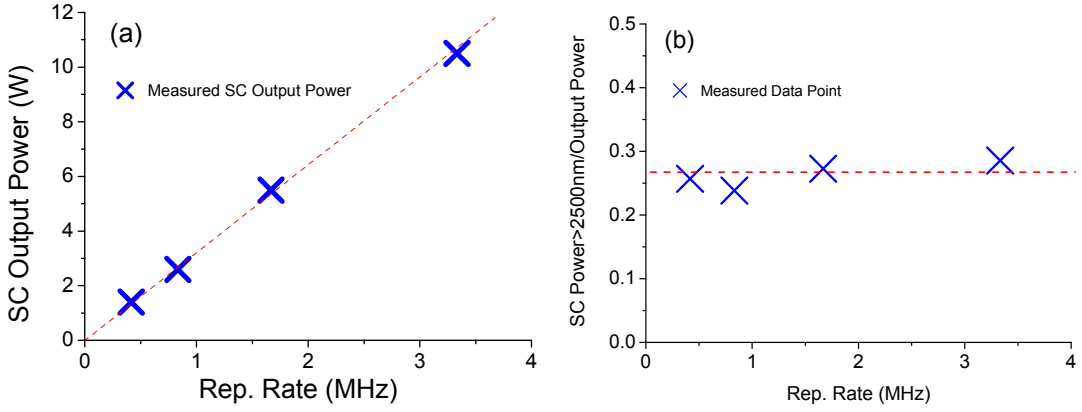

Fig. 4. (a)Average SC output power scaling by varying pulse repetition rate and pump power, (b) ratio of the SC power of the spectral components beyond 2500 nm with respect to total SC power under different operating repetition rate.

4. PULSE PATTERN MODULATION OF THE SC LIGHT SOURCE

We demonstrate pulse pattern modulation of our SC source by directly modulating the seed laser diode and controlling the signal gain of the power amplifier. To modulate the SC output, the optical pump pulses amplified by the multi-stage fiber amplifiers need to be temporally encoded with the desirable pulse pattern. However, constant input power level is required to saturate the amplifier during the time period of the SC-off coding pattern to prevent storage of excess energy in the EYFA that would otherwise damage the amplifier [21].

We modulate the SC output, i.e. turn the SC output on/off, by feeding pump pulses that are temporally patterned with high/low peak power to the ZBLAN fiber. SC generation is a nonlinear optical process, thus the broadband SC spectrum can only be generated by amplified laser diode pulses with sufficient peak power, which typically needs to be in the kilowatt range. Figure 5 illustrates an exemplary pump pulse pattern, where a "1" code represents the one SC-on pulse and a "0" code represents a series of SC-off mini-pulses. To enable the SC output, a high peak power bearing pump pulse can be coupled into the ZBLAN fiber to generate the broadband spectrum. On the other hand, a series of mini-pulses with low peak power, which undergo minimal nonlinear broadening in the ZBLAN fiber, are used to nullify the SC output. Therefore, the SC output can be directly modulated by temporally encoding the pulse pattern onto the driving currents for gain-switching DFB seed laser diodes.

We use mini-pulses during the SC off time period to saturate the power amplifier and maintain the same signal gain level for the succeeding SC-on pump pulses. In order to keep the gain of the power amplifier the same for both SC-on pump pulses and SC-off mini-pulses, the average output power of the pre-amplifier needs to stay unchanged. We use a feedback loop technique to continuously sample the output power of the pre-amplifier and then adjust the DFB seed laser power level accordingly to maintain constant output power. The 1% optical tap for signal strength monitoring is placed after the pre-amplifier and the bandpass filter, but before any of the middle stage amplifier components. This allows the signal to be strong enough that a 1% coupling still has a high signal-to-noise ratio (SNR) but avoids any significant nonlinear effects in the fiber and keeps detector saturation to a minimum. Placing the 1% tap after the OADM filter assures that the signal seen by the feedback loop and the middle stage amplifier are nearly identical, since the seed laser diode puts out a much higher percentage of power into wavelengths other than 1542 nm for the mini-pulses that are barely above threshold than it does for the main pump pulses. In particular, the pulse repetition rate is set to 1.54 MHz for the SC-on pump pulses and is switched to 50 MHz for the SC-off mini-pulses. Since the average power of the amplifier system remains unchanged, the peak power for the mini-pulse is reduced to <1/30 that of the normal pump pulse.

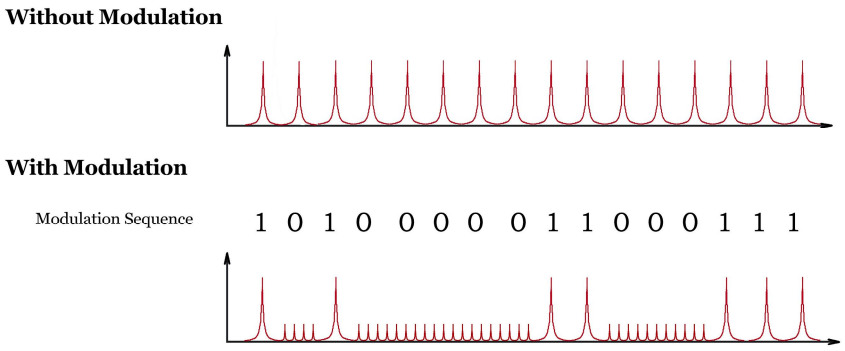

Fig. 5 Pump pulse modulation pattern (not drawn to scale). "0"/"1" represents SC off/on code.

Figure 6(a) shows a sample modulation pattern output of our SC source. The SC laser is operated at a base repetition rate of 1.54 MHz with pump pulse duration of 400 ps. The output power of the SC is measured to be ~2.4 W un-modulated. Two pulse envelops are encoded into the SC output—one has a width of 130 μs repeating at 1.5 kHz and the other has a width of 650 μs repeating at 7.7 kHz. Therefore, the modulation pattern consists of a 200 pulse burst with a temporal duration of 130 μs, followed by a SC-off time of 130 μs, plus another 1000 pulse burst with a temporal duration of 650 μs, followed by a SC-off time of 650 μs. The resulting duty cycle is 50% of the nominal SC output with the 1.54 MHz continuous repetitive pulses. One thing to notice is that the pulse trace displayed in Fig. 6(a) shows a ~25% peak to peak

variation. We attribute such amplitude variation to the limited bandwidth and memory depth of the oscilloscope used in the experiments, which leads to under-sampling of each pulse in the train and uncertainties in the pulse to pulse variation measurement. We have also used a fast oscilloscope (500 MHz bandwidth) to measure the peak-to-peak energy variation on a single pulse in the fix repetition rate mode at 1550 nm and 2555 nm. The peak-to-peak power variation is estimated to be approximately 3%.

The modulated SC spectrum is plotted in Fig. 6(b) overlapping with the un-modulated spectrum. The SC spectrum shown in Fig. 6 is generated in FL#2 and has similar spectral bandwidth as that generated in FL#1. The amplitude of the SC spectrum in the modulation mode in Fig. 6 is vertically displaced to match the SC spectrum in the un-modulated mode. We observe no discernible changes in the SC spectrum in both the long and short wavelength side. The spectral power remaining in the vicinity of the pump wavelength in the modulation mode is ~10 dB higher than that of un-modulated mode, which could be attributed to the optical power of the SC-off mini-pulses. The modulated SC outputs 3.45 W in total, within which ~1.2 W is estimated to be in the continuum. The measured modulated SC output correlates to the powers in the un-modulated mode with the 50% duty cycle. The residual power, i.e. 3.45 W-1.2 W, is composed of ~1 W remaining in the pump and the rest of the power representing spectral components with small wavelength shifting in the vicinity of pump wavelength. Future work will be conducted to increase the SC-off pulse repetition rate beyond 100 MHz to further reduce the peak power of the mini-pulses and the corresponding nonlinear wavelength shifting.

The modulation duty cycle of our SC laser can be adjusted from nominally 0% to 100%. We estimate the saturation time of the power amplifier is ~10 μs. As previously mentioned, a series of mini-pulse are injected into the power amplifier at the SC-off period to maintain the constant average output power of the amplifier. The switching time between regular pump pulse and mini-pulse is ~100-150 ns in our driving circuits for the seed laser diode. We also observe a slight "ramp up" region at the start of each pulse envelop in Fig. 6(a) which is due to the transient laser diode driver circuit response.

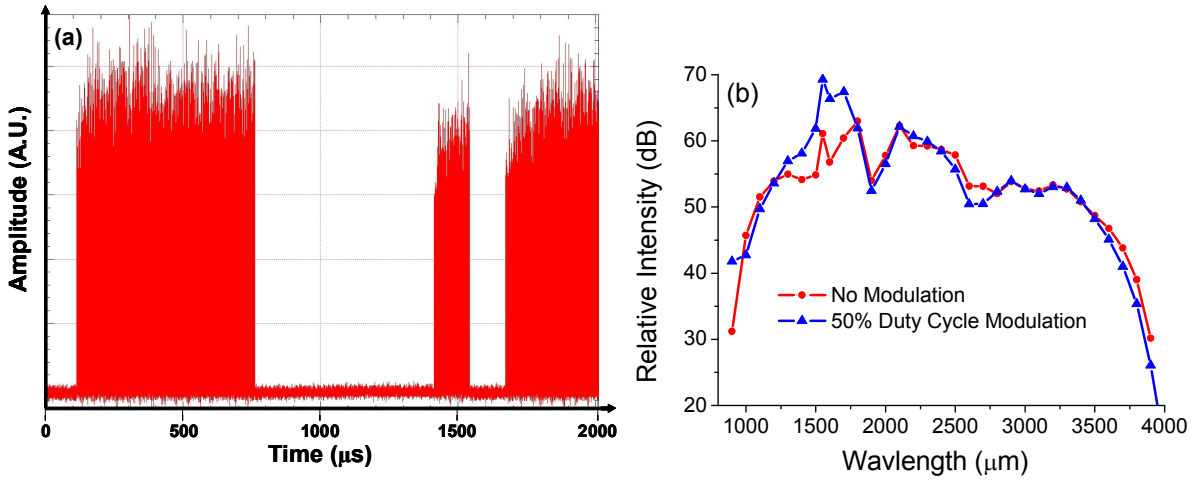

Fig. 6 SC modulation experiments: (a) output pulse modulation pattern. The modulation pattern consists of a 200 pulse burst with a temporal duration of 130 μs, followed by a SC-off time of 130 μs, plus another 1000 pulse burst with a temporal duration of 650 μs, followed by a SC-off time of 650 μs. (b) SC spectral output in modulated and un-modulated modes.

Our SC light source outputs near diffraction-limited beam quality over the entire spectrum. To measure the beam quality of the SC spectrum, the output of the SC is first collimated by a gold-coated parabolic reflective mirror and passes through optical bandpass filters in different bands. The filtered SC light is then focused by a CaF_2 lens and the intensity profile of the laser beam is mapped at difference axial locations around the focal spot by using a knife edge cutting across the beam. We estimate the M^2 value by fitting the beam shape to the Gaussian beam propagation profile. Figure 7 demonstrates the M^2 measurement of the SC output beam centered at (a) 1550 nm (~10 nm bandwidth), (b) 2555 nm (~50 nm bandwidth), and (c) 3275 nm (~50 nm bandwidth), all in FL#2. The generated SC spectrum is similar to that of FL#1 with the detailed spectrum analyzed in the following section. As can been seen, all of the wavelengths exhibit near

diffraction limited performance with M^2 approaching 1 moving towards the long wavelength region. Such behavior could be attributed to the step-index geometry of the ZBLAN fiber, which is not strictly single spatial mode at wavelengths below the cut-off wavelength (e.g. ~2.7 μm for FL#2). The M^2 value at 3275 nm is ~0.1 higher than that at 2555 nm, which might be due to the uncertainty of the measurement or the different filter bandwidth at these two wavelengths. It should also be noted that the output of the ZBLAN fiber is end-capped with a thin ZBLAN glass slide to prevent the surface damage, which might also reduce the output beam quality of the SC at various wavelengths.

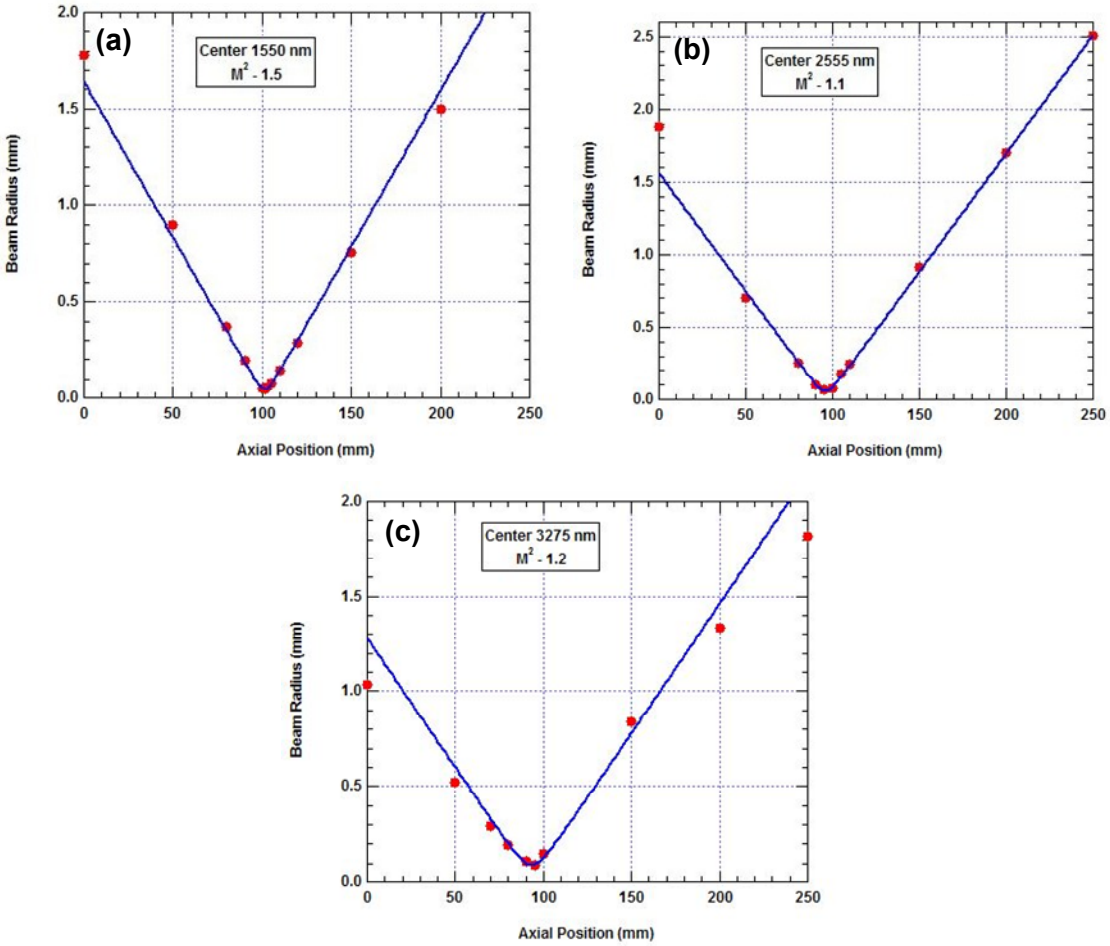

Fig. 7 Beam quality M^2 measurement at (a) 1550 nm (b) 2555 nm (c) 3275 nm.

5. ABSORPTION SPECTROSCOPY AND SELECTIVE ABLATION OF LIPIDS

As one example of the application of the MIRFIL to bio-photonics, we examine the spectroscopy and selective ablation of the constituents of vulnerable plaque. In the mid-infrared (mid-IR) region between 2.6-3.8 μm, lipids and proteins have fundamental absorptions that lie at different wavelengths. Therefore, we exploit the difference in spectral features for potential diagnostics or therapeutics for ailments associated with lipid-rich tissues. Selective ablation is possible because proteins show primary light absorption at 2.8-3.2 μm due to N-H and O-H bonds, while lipids exhibit absorptions in 3.2-3.6 μm associated with C-H stretching vibrations. We use absorption spectroscopy to identify or differentiate the constituents of atherosclerotic plaque from smooth muscle cells or endothelial cells. In addition, by using light in 3.2-3.6 μm that targets the lipid absorption lines, we selectively ablate lipid-rich samples such as adipose tissue without damaging normal aorta.

The fiber based SC laser source provides a new platform for spectroscopy measurements and tissue ablations in the mid-IR. Mid-IR absorption spectra of the atherosclerotic plaque components, including adipose tissue, macrophages and foam cells, have been measured by both a lamp based [22] and a synchrotron laser [23] based FTIR system. On the other hand, single wavelength-dependent selective ablation has been performed in 5.75 μm to 6.1 μm for ablation of cholesterol esters using free-electron laser [24]. In comparison, our all-fiber-integrated light source has been packaged into a 2U rack unit (19 inches in width/21 inches in depth/4 inches in height), and the MIRFIL could be potentially deployed in the clinical environment for practical medical use.

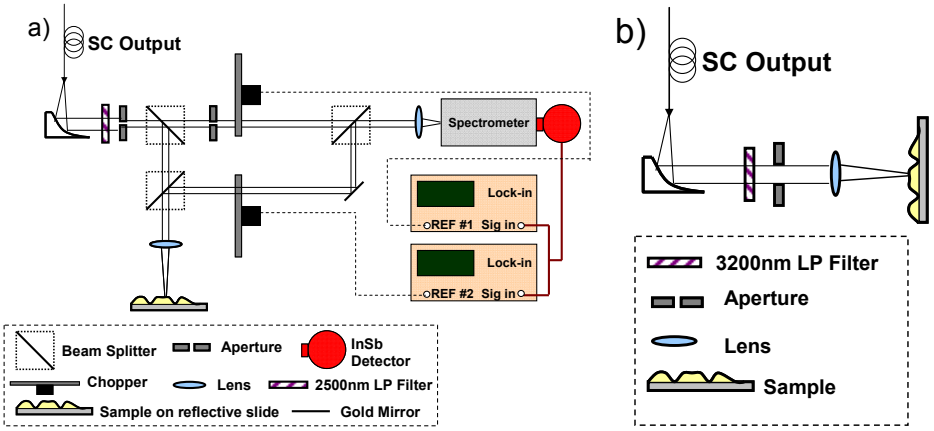

Fig. 8. a) Reflection-absorption spectra measurement setup. b) Selective laser ablation setup.

The experimental setup comprises three parts—the SC laser, mid-IR spectroscopy, and laser ablation. For absorption spectrum measurements, the output of the SC laser is coupled to the mid-IR spectroscopy setup as illustrated in Fig. 8a. To improve the signal-to-noise ratio of the measurements, the SC light is first collimated by a parabolic mirror and then split into one signal arm that passes through the sample under test and one reference arm. The two beams are modulated by optical choppers at different frequencies. The recombined SC light is coupled into a grating-based spectrometer with signal collected by a liquid-nitrogen cooled InSb detector. For selective ablation, the SC light residing in the lipids vibrational bands is selected out by a ~3200 nm long pass filter (Fig. 8b). The filtered light is then focused by a 25.4 mm CaF_2 lens to a spot size to ~3 mm onto the sample. Spectroscopy and ablation are performed *in vitro* on both tissue samples and cultured cells.

We measure mid-IR reflective absorption spectra of the constituents of atherosclerotic plaque and normal artery in the 2.6-3.8 μm regime (Fig. 9a). As an example, a broad absorption feature in 2.8-3.2 μm is observed in the protein-rich samples, including artery compositions—endothelial cells and smooth muscle cells, as well as macrophages. Such feature can be attributed to the vibrational bands of O-H stretching in the hydroxyl group and N-H stretching present in the protein peptides [23,25]. In contrast, the fatty lipid sample demonstrates absorption lines in the 3.2-3.6 μm window, including =CH stretching at ~3330 nm, CH_3 at ~3390 nm, and CH_2 at ~3420 nm and ~3510 nm [25]. In addition, prominent spectral characters between ~3.2 to 3.6 μm with two absorption peaks at ~3420 nm and ~3510 nm are observed in the foam cells, revealing the pathological relationship between these two cell types, i.e. active macrophages engulfing lipid-rich substance to grow into foam cells.

We perform selective ablation of adipose tissue in comparison to artery wall (Fig. 9b). We hypothesize that by targeting the laser to the 3.2-3.6 μm lipid absorption band we can heat adipose tissue to a damage threshold faster than artery tissue. Selective ablation, i.e. preferentially heating of adipose tissue without damaging artery tissue, is observed under light microscopy with a SC laser fluence starting as low as ~15 mJ/mm^2. We also conduct histology to examine biological integrity of the artery tissues (Fig. 9c). While laser induced damage can be observed at a laser fluence of ~102 mJ/mm^2, no such effects are present at ~33 mJ/mm^2 and very subtle wounds exist at ~72 mJ/mm^2.

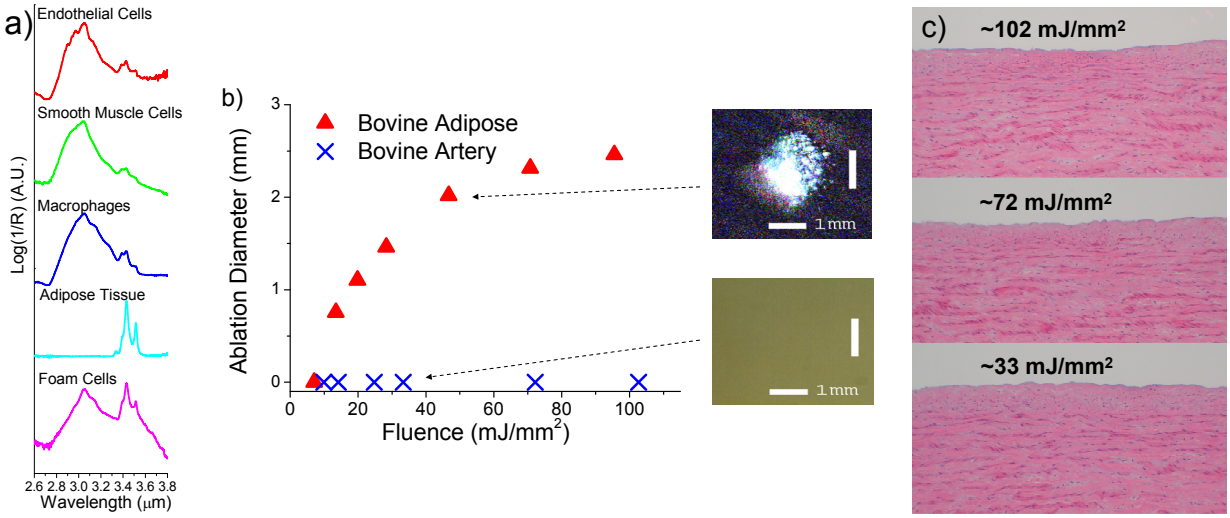

Fig. 9. a) Absorption spectra of normal artery and atherosclerotic plaque compositions taken with SC laser. b) Left, power dependence of the ablation diameter in adipose tissue and bovine artery. Right, images showing the difference before and after ablation at ~40 mJ/mm^2. c) Histology of adipose tissue under various laser fluence.

The absorption spectra acquired by our SC laser are consistent with the measurements conducted by the thermal lamp and synchrotron laser based system [22-24]. We measure the absorption spectra by using a SC average power of <1 mW and scale up the power to the range of 20-200 mW for ablation experiments. In addition, while optical microscopy is sufficient to track the melting of the adipose tissue, histology is required to reveal the minute damage in the artery tissues.

Thus mid-IR absorption spectra of normal artery and atherosclerotic plaque compositions are measured by using an all-fiber-integrated SC laser source. Distinctive spectral signatures in 3.2-3.6 μm range associated with fatty acids and cholesterol esters absorptions are present in foam cells and adipose tissues. On the other hand, normal artery and macrophages have dominant features at 2.8-3.2 μm, corresponding to protein and water absorption. Selective ablation of the lipid-rich adipose tissue is demonstrated by using the SC laser to target the 3.2-3.6 μm C-H stretching vibration band under laser fluence ranging from ~15 mJ/mm^2 to ~33 mJ/mm^2.

6. DISCUSSION AND CONCLUSION

The all-fiber-integrated configuration improves the mechanical stability and the power efficiency of our SC light source. In the previous high power SC experiments [20], we have used an erbium/ytterbium co-doped cladding-pumped fiber laser with bulk optical coupling between different stages of the amplifier. The power efficiency from the pump diodes to the output in the SMF is ~14%. In comparison, by splicing the amplifier stage together and removing the bulk optics, the pump-to-output efficiency is more than doubled to ~30%. Under normal operation, the pump diode wall-plug electrical-to-optical efficiency is about 50% and the pump-to-SC conversion efficiency is ~50% as discussed earlier. Therefore, the wall-plug electricity-to-SC power efficiency, defined as the ratio of the generated SC average power out of the total electrical power consumption is improved to >7% for our SC light source from <3% for the table-top system. To further improve the overall power efficiency of the system, the coupling efficiency of the mechanical splice needs to be increased, e.g. adding an intermediate fiber to better match the mode profile of the SMF and ZBLAN fibers. Moreover, the pump diodes of the last stage power amplifiers can be turned off during the long SC-off period in the modulated scenario to save the wall-plug electricity consumption.

Our SC light source is scalable in the time-averaged power up to 10.5 W by changing the pulse repetition rate. We show in Fig. 4 that the SC average power can be continuously varied by a factor of 7.5, i.e. from 1.4 W to 10.5 W, by increasing the pulse repetition rate by the same scale from 0.42 MHz to 3.33 MHz and increasing the pump power supply correspondingly. The power scalability is enabled by using the amplified laser diode pulses as the pump source for the SC generation. Compared to the conventional mode-locked lasers, our SC laser has a greater flexibility in the

system configuration from the mature telecommunication technology and has potential scalability in the output power by adding more pump laser diodes.

In our experiments, the output time-averaged power is currently limited by the available pump power diodes coupled to the fiber amplifier. As a rule-of-thumb, one 8 W pump diode contributes ~1 W average power to the SC generation. Therefore, we use twelve 8 W pump diodes in our pump system to generate the SC with ~10.5 W output power. To further scale up the SC average power, more pump diodes need to be used to feed the fiber amplifier to generate a higher pump power. To further extend the SC long wavelength edge, new infrared optical fiber, such as tellurite fiber, needs to be used. For example, SC generation extending to ~5 μm is demonstrated in a tellurite fiber with photonic crystal structure [16].

In summary, mid-IR SC with 10.5 W time-averaged power and a continuous spectrum of ~0.8-4 μm is generated in ZBLAN fibers by amplified nanosecond diode pulses. The average output power of the SC is linearly scalable from 1.4 W to 10.5 W while maintaining the similar spectra by varying input pump power and the corresponding pulse duty cycle. We demonstrate modulation of the SC output pulse at 50% duty cycle with 1.5 kHz and 7.7 kHz modulation speed by directly modulating the seed laser diode and controlling the amplifier gain. As one example of the application of the mid-IR SC, we perform spectroscopy and selective ablation on the constituents of atherosclerotic plaque and compare with normal arteries.

Acknowledgment

This work was supported in part by Army Research Office under project W911NF-04-C-0078, in part by Defense Advanced Research Projects Agency (DARPA) under project W31P4Q-05-C-0159, and in part by Omni Sciences, Inc. Some of the laboratory equipment for this work was funded by Vyalex Inc. through a contract from the Naval Air Command (NAVAIR) PMA-272. Mohammed N. Islam is also Founder and Chief Technology Officer of Omni Sciences, Inc.

REFERENCES

[1] R. R. Alfano, The supercontinuum laser source: fundamentals with updated references, 2nd ed. (Springer, New York, 2006).

[2] T. Morioka, K. Mori, S. Kawanishi, and M. Saruwatari, “Multi-WDM-channel, GBit/s pulse generation from a single laser source utilizing LD-pumped supercontinuum in optical fibers,” IEEE Photon. Technol. Lett. **6**, 365-368 (1994).

[3] H. Takara, “Multiple optical carrier generation from a supercontinuum source,” Opt. Photon. News **13**, No. 3 48-51 (2002).

[4] F. G. Omenetto, N. A. Wolchover, M. R. Wehner, M. Ross, A. Efimov, A. J. Taylor, V. V. R .K. Kumar, A. K. George, J .C. Knight, N. Y. Joly, and P. St. J. Russell, “Spectrally smooth supercontinuum from 350 nm to 3 μm in sub-centimeter lengths of soft-glass photonic crystal fibers,” Opt. Express **14**, 4928-4934 (2006).

[5] C. Xia, M. Kumar, M. Y. Cheng, O.P. Kulkarni, M. N. Islam, M. N, A. Galvanauskas, F. L. Terry, M. J. Freeman, D. A. Nolan, and W. A. Wood, "Supercontinuum Generation in Silica Fibers by Amplified Nanosecond Laser Diode Pulses," IEEE J. Sel. Top. Quantum Electron **13**, 789-797 (2007).

[6] T. Izawa, N. Shibata, and A. Takeda, “Optical attenuation in pure and doped fused silica in their wavelength region,” App. Phys. Lett. **31**, 33-35 (1977).

[7] J. C. Travers, A. B. Rulkov, B. A. Cumberland, S. V. Popov, and J. R. Taylor, "Visible supercontinuum generation in photonic crystal fibers with a 400W continuous wave fiber laser," Opt. Express **16**, 14435-14447 (2008).

[8] I. T. Sorokina and K. L. Vodopyanov, eds., *Solid-State Mid-Infrared Laser Sources*, (Springer-Verlag, Berlin Heidelberg, 2003).

[9] M. Razeghi, S. Slivken, Y. Bai, and S. R. Darvish, “The quantum cascade laser: a versatile and powerful tool,” Opt. Photon. News **19**, No. 7 42-47 (2008).

[10] K. Wille, “Synchrotron radiation sources,” Rep. Prog. Phys. **54**, 1005-1067 (1991).

[11] G. S. Edwards, R. H. Austin, F. E. Carroll, M. L. Copeland, M. E. Couprie, W. E. Gabella, R. F. Haglund, B. A. Hooper, M. S. Hutson, E. D. Jansen, K. M. Joos, D. P. Kiehart, I. Lindau, J. Miao, H. S. Pratisto, J. H. Shen, Y. Tokutake, A. F. G. van der Meer, and A. Xie, “Free-electron-laser-based biophysical and biomedical instrumentation,” Rev. Sci. Instrum. **74**, 3207-3245 (2003).

[12] R. R. Anderson, W. Farinelli, H. Laubach, D. Manstein, A. N. Yaroslavsky, J. Gubeli, K. Jordan, G. R. Neil, M. Shinn, W. Chandler, G. P. Williams, S. V. Benson, D. R. Douglas, H. F. Dylla, "Selective photothermolysis of lipid-rich tissues: A free electron laser study," Lasers in Surgery and Medicine **38**, 913-919 (2006).

[13] J. Mandon, E. Sorokin, I. T. Sorokina, G. Guelachvili, and N. Picqué, "Supercontinua for high-resolution absorption multiplex infrared spectroscopy," Opt. Lett. **33**, 285-287 (2008).

[14] S. A. Diddams, D. J. Jones, J. Ye, S. T. Cundiff, J. L. Hall, J. K. Ranka, R. S.Windeler, R. Holzwarth, T. Udem, and T.W. Hänsch, "Direct link between microwave and optical frequencies with a 300 THz femtosecond laser comb," Phys. Rev. Lett. **84**, 5102–5104 (2000).

[15] C. L. Hagen, J. W. Walewski, and S. T. Sanders, "Generation of a continuum extending to the midinfrared by pumping ZBLAN fiber with an ultrafast 1550-nm source," IEEE Photon. Technol. Lett. **18**, 91-93 (2006).

[16] P. Domachuk, N. A. Wolchover, M. Cronin-Golomb, A. Wang, A. K. George, C. M. B. Cordeiro, J. C. Knight, and F. G. Omenetto, "Over 4000 nm bandwidth of mid-IR supercontinuum generation in sub-centimeter segments of highly nonlinear tellurite PCFs," Optics Express **16**, 7161-7168 (2008).

[17] O. P. Kulkarni, C. Xia, D. J. Lee, M. Kumar, A. Kuditcher, M. N. Islam, F. L. Terry, M. J. Freeman, B. G. Aitken, S. C. Currie, J. E. McCarthy, M. L. Powley, and D. A. Nolan, "Third order cascaded Raman wavelength shifting in chalcogenide fibers and determination of Raman gain coefficient," Opt. Express **14**, 7924-7930 (2006).

[18] J. S. Sanghera, L. B. Shaw, C. M. Florea, P. Pureza, V. Q. Nguyen, D. Gibson, F. Kung, and I. D. Aggarwal, "Non-linearity in chalcogenide glasses and fibers, and their applications," presented at Quantum Electronics and Laser Science Conference QELS 2008, San Jose, Calif., May 4-9, 2008, QTuL5.

[19] C. Xia, M. Kumar, O. P. Kulkarni, M. N. Islam, F. L. Terry, Jr., M. J. Freeman, M. Poulain, and G. Mazé, "Mid-infrared supercontinuum generation to 4.5 μm in ZBLAN fluoride fibers by nanosecond diode pumping," Opt. Lett. **31**, 2553-2555 (2006).

[20] C. Xia, M. Kumar, M. -Y. Cheng, R. S. Hegde, M. N. Islam, A. Galvanauskas, H. G. Winful, F. L. Terry, Jr., M. J. Freeman, M. Poulain, and G. Mazé, "Power scalable mid-infrared supercontinuum generation in ZBLAN fluoride fibers with up to 1.3 watts time-averaged power," Opt. Express **15**, 865-871 (2007).

[21] G. Canat, J. Mollier, J. Bouzinac, G. M. Williams, B. Cole, L. Goldberg, Y. Jaouën, and G. Kulcsar, "Dynamics of high-power erbium–ytterbium fiber amplifiers," J. Opt. Soc. Am. B **22**, 2308-2318 (2005).

[22] B. A. Hooper, A. Maheshwari, A. C. Curry, and T. M. Alter, "Catheter for diagnosis and therapy with infrared evanescent waves," Appl. Opt. **42**, 3205-3214 (2003).

[23] H. –Y. N. Holman, K. A. Bjornstad, M. C. Martin, W. R. Mckinney, E. A. Blakely, and F. G. Blankenberg, "Mid-infrared reflectivity of experimental atheromas," J. Biomed. Opt. **13**, 030503 (2008).

[24] K. Awazu, A. Nagai, and K. Aizawa, "Selective removal of cholesterol esters in an arteriosclerotic region of blood vessels with a free-electron laser," Lasers in Surgery and Medicine **23**, 233-237 (1998).

[25] C. Paluszkiewicz, W. M. Kwiatek, A. Banas, A. Kisiel, A. Marcelli, and A. Piccinini, "SR-FTIR spectroscopic preliminary findings of non-cancerous, cancerous, and hyperplastic human prostate tissues," Vibrational Spectroscopy **43**, 237-242 (2007).